UNIVERSITY OF OKLAHOMA

GRADUATE COLLEGE

METABOLITE PROFILING OF EXPERIMENTAL CUTANEOUS LEISHMANIASIS LESIONS DEMONSTRATES SIGNIFICANT PERTURBATIONS IN TISSUE GLYCEROPHOSPHOCHOLINES

A THESIS

SUBMITTED TO THE GRADUATE FACULTY

in partial fulfillment of the requirements for the

Degree of

MASTER OF SCIENCE

By

ADWAITA PARAB
Norman, Oklahoma
2021

METABOLITE PROFILING OF EXPERIMENTAL CUTANEOUS LEISHMANIASIS LESIONS DEMONSTRATES SIGNIFICANT PERTURBATIONS IN TISSUE GLYCEROPHOSPHOCHOLINES

A THESIS APPROVED FOR THE DEPARTMENT OF MICROBIOLOGY AND PLANT BIOLOGY

BY THE COMMITTEE CONSISTING OF

Dr. Laura-Isobel McCall

Dr. Elizabeth Karr

Dr. Krithivasan Sankaranarayanan

Table of Contents

Abstract

Each year 700,000 to 1.2 million new cases of cutaneous leishmaniasis (CL) are reported and yet CL remains one of thirteen diseases classified as neglected tropical diseases (NTDs). *Leishmania major* is one of several different species of that same genus that can cause CL. Current CL treatments are limited by adverse effects and rising resistance. Studying disease metabolism at the site of infection can lead to new drug targets. In this study, samples were collected from mice infected in the ear and footpad with *L. major* and analyzed by untargeted liquid chromatography-tandem mass spectrometry (LC-MS/MS). Significant differences in overall metabolite profiles were noted in the ear at the site of the lesion. Interestingly, lesion-adjacent, macroscopically healthy sites also showed alterations in specific metabolites, including select phosphocholines (PCs). Host-derived PCs in the lower *m/z* range (*m/z* 200-799) showed an increase with infection in the ear at the lesion site, while those in the higher *m/z* range (*m/z* 800-899) were decreased with infection at the lesion site. Overall, our results expanded our understanding of the mechanisms of CL pathogenesis through the host metabolism and may lead to new curative measures against infection with *Leishmania*.

Chapter 1: Introduction

Leishmaniasis affects people in 88 countries worldwide in tropical, subtropical and temperate regions, putting approximately 350 million individuals at risk of infection, with approximately 12 million battling the disease [1]. It is one of the three most impactful vector-borne protozoan neglected tropical diseases, causing approximately 2.1 million DALYs (Disability-Adjusted Life Years) and 51,000 deaths annually. With recent population movements, leishmaniasis is now affecting people in non-endemic regions as well. The expanding spread of leishmaniasis can be attributed to climate change and social constraints of populations living in poverty and conflict. Leishmaniasis is a disease that is exacerbated by poverty and socio-economic barriers, increasing rates of disease progression, mortality and morbidity and with significant social stigma [2][3].

Leishmaniasis is caused by about 20 different species of the parasite *Leishmania,* with three clinical syndromes: visceral, cutaneous (CL) and mucocutaneous leishmaniasis. CL is the most common form of the disease and symptoms include skin lesions and ulcers on exposed parts of the body. Mucocutaneous leishmaniasis is a disabling form where the lesions can lead to destruction of soft tissue of the nose, mouth and throat cavities. Of the three clinical forms of the disease, visceral leishmaniasis (kala-azar) is the deadliest, with serious symptoms like swelling of the liver and spleen, extreme anemia and frequent bouts of fever. Infection is transmitted through female sandflies of the *Phlebotomus* genus in the Old World and *Lutzomyia* genus in the New World [4]. Promastigotes enter the body upon being bitten by a female sandfly. They are taken up by macrophages, where they enter the amastigote stage, multiplying and affecting various tissue types depending on whether infection is initiated by a viscerotropic or dermotropic parasite strain [5][6]. This initiates the clinical manifestations of the disease. Humans as well as other mammals serve as host reservoirs for the parasite [7].

The current course of treatment for CL is usually antimonial drug compounds. These are known to be highly toxic compounds, in addition to the threat of increased parasite resistance to antimony in several regions of the world. Miltefosine, amphotericin B and paromomycin are among the other drugs that are administered for CL treatment, all of which have the drawbacks of high level of toxicity, increased drug resistance and treatment failure. Miltefosine is also teratogenic and should not be given to women in childbearing age. Treatment failure can be attributed to the characteristics of the host (immune system and nutritional status), of the parasite (mechanisms of survival within the host, drug resistance mechanisms, tissue location, etc.) and environmental factors such as awareness and treatment accessibility [8]. Approaching disease pathogenesis from a molecular perspective could uncover new mechanisms of infection and aid in developing new cures for leishmaniasis [9].

Alongside genes and proteins, metabolites play an important role in the life of an organism. The metabolome reflects the true functional endpoint of a complex biological system and provides a functional view of the organism by taking into account the sum of its genes, RNA, proteins and its environment [10]. Untargeted metabolomics can help identify metabolites involved in disease pathogenesis, in an unbiased fashion, acquiring data across a broad mass range [11]. For example, untargeted metabolomics has shown that miltefosine's mode of action *in vitro* may be related to modulation of parasite lipid metabolism, particularly

increased levels of by-products of lipid turnover [12]. The overall aim of this work was to perform an untargeted metabolic analysis of CL lesions in mice infected with *Leishmania major*. Our results showed significant changes in the host metabolism, specifically glycerophosphocholines (PC), in the skin lesions of CL.

Chapter 2: Results

To better understand the impact of infection on tissue metabolites, we analyzed overall and specific metabolite differences in the presence and absence of infection with *Leishmania major,* at sites of lesion and lesion-adjacent sites (with no visible signs of infection). BALB/c mice were injected intradermally in the ear. Eight weeks post-infection, samples were collected from the area where the parasites were injected, which showed skin lesions ("infected ear center"), the surrounding area that appeared infection-free ("infected ear edge"), and the matched tissue regions from the uninfected ear ("uninfected ear center", "uninfected ear edge") (Figure 1A). Metabolites were extracted with aqueous and organic solvents and analyzed by untargeted LC-MS/MS (see Materials and Methods). Overall, for both aqueous and organic extractions, distinct global metabolite profiles were observed by Principal Coordinate Analysis (PCoA) for the infected ear center compared to infected ear edge (PERMANOVA $p<0.01$, aqueous extraction $R^2 = 0.743$, organic extraction $R^2= 0.643$), to uninfected ear center (PERMANOVA $p<0.01$, aqueous extraction $R^2=0.739$, organic extraction $R^2=0.805$) and to uninfected ear edge (PERMANOVA $p<0.01$, aqueous extraction $R^2=0.288$, organic extraction $R^2=0.248$). In contrast, no significant differences for both aqueous and organic extracts by PCoA analysis in terms of overall metabolite profile were observed between infected ear edge and uninfected ear samples (Figure 1B and 1C, PERMANOVA $p>0.1$). Thus, *L. major* infection changes the overall tissue chemical composition at the lesion location in the ear. In contrast, the impact of *L. major* infection on overall footpad metabolite profile for the organic (PERMANOVA $p=0.218$ $R^2=0.156$) and aqueous (PERMANOVA $p=0.244$ $R^2=0.146$) extractions was much more minor. Random forest machine learning analysis [13] was performed to identify the metabolites most affected by infection in both experimental systems, with annotation performed using molecular networking and GNPS [14]. Annotatable molecules most highly affected by infection include metabolites of the phosphocholine (PC) family of phospholipids, glutamine, and eicosatrienoic acid (Table 1, 2, 3, 4, Figure S1). Glutamine was decreased with infection at the site of the ear lesion (Wilcoxon rank sum test p value=0.0079 comparing to uninfected ear center), although it was unaffected by infection in the footpad. Eicosatrienoic acid was increased in the infected footpad (Wilcoxon rank sum test p value=0.0079).

Given that many of the differential molecules are PCs, we investigated the impact of infection on this family in greater detail. Molecular network analysis of PC family molecules in both aqueous and organic ear extracts showed that most detected PCs were strongly increased by infection (Fig 1 D, S2 Fig). In particular, the infected group was significantly higher than the uninfected group for PCs in the lower ranges of *m/z* 200-299, 400-499, 500-599, and 600-699 (Wilcoxon rank sum test p value<0.05). These were also significantly higher in the infected ear center compared to infected ear edge, to uninfected ear center, and to uninfected ear edge (Wilcoxon rank sum test p value<0.05 for each pairwise comparison, Fig 1 E, F). In the range of *m/z* 700-799, the levels of PCs in the infected ear center were significantly greater than in the uninfected ear center (Wilcoxon rank sum test p value < 0.05) (Fig 1 I). A reverse trend was observed in the mass range of *m/z* 800-899 where the PC levels were significantly higher in the uninfected ear center in comparison to the infected ear center (Wilcoxon rank sum test p value < 0.05) (Fig 1J). No PCs were detected in the *m/z* 300-399 range. Total PCs were significantly increased in the infected group in comparison to the uninfected group (Wilcoxon rank sum test p value<0.05, Fig 1 K). Given that all these PCs were detected in both infected and uninfected

samples, albeit at differential abundances, they are either host-derived or commonly produced by both parasite and host. Likewise, most PCs were increased by infection in the footpad (Table 3, 4, S2 Fig). These results indicate that PCs are strongly affected by cutaneous *Leishmania* infection. In addition, our observation that specific PCs as well as PCs of multiple *m/z* ranges are also affected at lesion-adjacent sites ("infected ear edge") indicates that infection-induced metabolic perturbations are not restricted to the lesion site, revealing a better picture of what is happening to the host during the disease state and providing clues to the pathways involved.

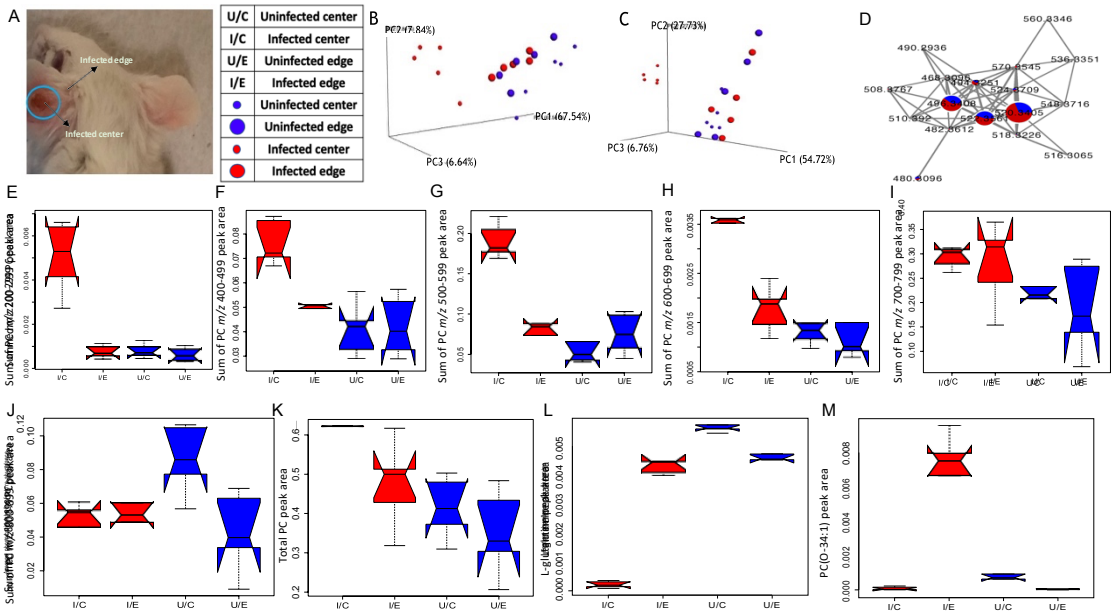

Figure 1. Effect of in vivo L. major infection on host metabolite profile. (A) Sites of infection and sample collection. Lesion at the center of the infected ear is circled in blue. (B) PCoA analysis of aqueous extraction from infected and uninfected ear samples, showing overall differences in metabolite profiles between sampling sites. PERMANOVA p= 0.004, R2=0.288. (C) PCoA analysis of organic extraction from infected and uninfected ears, showing differences in global metabolite profiles between sampling sites. PERMANOVA p= 0.003, R2=0.248. (D) Representative subnetwork of phosphocholine (PC) molecular family members found in ear tissue and showing high relative abundance with infection (red) and low abundance without infection (blue). Nodes are scaled by normalized feature peak area. (E-J) PCs in the m/z range 200-299, 400-499, 500-599, 600-699, 700-799 and 800-899, respectively, change with infection and sampling position in the ear. (K) Total PC levels were increased at the site of infection in the ear. (L) Representative metabolite decreased by infection at the site of the lesion: glutamine (Wilcoxon rank-sum test comparing infected ear center vs infected ear edge p=0.007937). (M) Representative metabolite increased only at infection-adjacent sites: PC(O-34:1), Wilcoxon rank-sum test comparing infected ear center vs infected ear edge p=0.007937). Non-overlapping boxplot notches indicate significantly different medians between groups.

m/z	**RT (min)**	**Spectral match on GNPS / LIPID MAPS / Molecular networking**	**Mass difference**	**PPM error**	**Cosine score**	**Number of matched peaks**	**Impact of infection in ear**	**P value (infected center vs uninfected center)** [1]	**P value (infected edge vs uninfected edge)**	**P values (infected vs uninfected)**	**Impact of infection in footpad (Aqueous extraction)**	**Impact of infection in footpad (Organic extraction)**
794.60551	4.42	PC 20:3/18:1	0	0	0.82	5	High in infected ear edge	0.056	0.008	0.481	ND	High in infected
772.62001	4.73	PC O-36:2	NA[2]	1.8	NA	NA	High in infected ear edge	0.016	0.008	0.393	ND	ND[3]
750.54335	5.06	NA	NA	NA	NA	NA	High in infected ear center	0.008	0.008	2.17E-05	ND	High in infected
155.04998	0.85	NA	NA	NA	NA	NA	High in infected & uninfected ear edges	0.008	0.222	0.684	ND	ND
752.55585	5.07	NA	NA	NA	NA	NA	High in infected ear center	0.008	0.008	1.08E-05	ND	Higher in infected

744.5906	4.48	LPC 34:2 or LPC O-34:3;O or PC O-34:2	NA	0.54	NA	NA	High in infected ear edge	0.008	0.008	0.052	ND	ND
746.6052	4.78	PC O-16:0/18:1	0	4	0.96	14	High in infected ear edge	0.032	0.008	0.280	ND	Higher in infected
796.6205	4.91	PC O-38:4	NA	1.26	NA	NA	High in infected ear edge	0.151	0.008	0.105	ND	Higher in infected
147.0815	0.34	Glutamine	0.01	78	0.87	4	Low in infected ear center	0.008	0.421	0.001	No difference noted	No difference noted
770.605	4.58	PC O-36:3	NA	1.04	NA	NA	High in infected ear edge	0.310	0.008	0.218	ND	ND
720.5887	4.7	LPC 32:0 or LPC O-32:1;O or PC O-32:0	NA	NA	NA	NA	High in infected ear edge	0.095	0.008	0.280	ND	ND
794.6052	6.13	PC 20:3/18:1	NA	2.08	NA	NA	High in infected ear center	0.008	0.008	1.08E-05	ND	High in infected

330.1314	6.4	NA	NA	NA	NA	NA	High in infected ear center	0.008	0.008	1.08E-05	ND	ND
169.0624	0.31	NA	NA	NA	NA	NA	Low in infected ear center	0.011	0.548	0.011	No difference noted	No difference noted
261.1474	0.47	NA	NA	NA	NA	NA	High in infected ear edge and uninfected ear edge	0.095	0.310	0.315	No difference noted	No difference noted

[1] Test returns identical p-values when non-overlapping peak areas are obtained between samples in each group (due to identical ranks regardless of the specific peak areas.)
[2] NA, not applicable
[3] ND, not detected

Table 2. Top differential molecules for ear organic extraction as determined by random forest

m/z	RT	Spectral match on GNPS	Mass difference	PPM error	Cosine score	Number of matched peaks	Impact of infection in ear	P values (inf center vs uninfected center)[1]	P values (inf edge vs uninfected edge)	P values (infected vs uninfected)	Impact of infection in footpad (Aqueous extraction)	Impact of infection in footpad (Organic extraction)
768.5862	5.26	PC O-36:4	NA[2]	5.2	NA	NA	High in infected ear center	0.008	0.008	1.08E-05	ND[3]	Higher in infected
792.5574	5.71	PC O-16:0/22:6	0.01	8	0.86	7	High in infected ear center	0.012	0.691	0.026	ND	No difference noted
856.5826	5.87	NA	NA	NA	NA	NA	High in uninfected ear center	0.008	1	0.105	ND	ND
856.5826	5.9	NA	NA	NA	NA	NA	High in uninfected ear center	0.008	0.841	0.075	ND	ND
813.6845	5.27	NA	NA	NA	NA	NA	High in infected ear edge	0.016	0.008	0.912	ND	Higher in infected

790.5424	5.43	PC 37:7	NA	5.44	NA	NA	High in infected ear center & uninfected ear center	0.548	0.691	0.631	ND	No difference noted
828.5516	5.44	PC O-40:10;O or PC 40:9	NA	1.2	NA	NA	High in uninfected ear center	0.008	0.691	0.143	ND	ND
854.5676	5.36	NA	NA	NA	NA	NA	High in infected ear center & uninfected ear center	0.056	0.222	0.218	ND	No difference noted
806.5682	5.42	PC 38:6 or PC O-38:7;O	0.02	22	0.81	18	High in uninfected ear center	0.008	1	0.09	ND	ND
834.5994	5.91	PC 40:6 or PC O-40:7;O	NA	1.56	NA	NA	High in uninfected ear center	0.008	0.548	0.353	ND	ND
1017.6873	3.04	NA	NA	NA	NA	NA	High in infecte	0.008	0.151	0.002	ND	ND

							d ear center					
770.6019	5.7	PC O-36:3	NA	5.06	NA	NA	High in infected ear center	0.008	0.095	0.0001	ND	ND
744.5848	5.59	LPC 34:2 or LPC O-34:3;O or PC O-34:2	NA	7.25	NA	NA	High in infected ear center	0.011	0.052	0.0003	ND	ND
332.6611	2.29	NA	NA	NA	NA	NA	High in uninfected	0.008	0.222	0.0003	ND	ND
377.2679	3.53	NA	NA	NA	NA	NA	High in infected ear center	0.008	0.222	0.043	No diference noted	ND

[1] Test returns identical p-values when non-overlapping peak areas are obtained between samples in each group (due to identical ranks regardless of the specific peak areas.)
[2] NA, not applicable
[3] ND, not detected

Table 3. Top differential molecules for footpad aqueous extraction as determined by random forest

m/z	**RT**	**Spectral match on GNPS / LIPID MAPS / Molecular networking**	**Mass difference**	**PPM error**	**Cosine score**	**Number of matched peaks**	**Impact of infection in footpad**	**P values[1]**	**Impact of infection in ear (Aqueous extraction)**	**Impact of infection in ear (Organic extraction)**
331.2638	4.31	NA[2]	NA	NA	NA	NA	High in infected	0.008	ND	ND
368.2591	4.06	Acylcarnitine family member	NA	NA	NA	NA	High in infected	0.008	ND	ND
377.1461	2.41	NA	NA	NA	NA	NA	High in infected	0.012	ND	ND
425.3375	3.18	NA	NA	NA	NA	NA	High in uninfected	0.008	ND	ND
210.1121	2.74	NA	NA	NA	NA	NA	High in uninfected	0.008	No difference noted	ND
212.1651	2.75	NA	NA	NA	NA	NA	High in uninfected	0.008	No difference noted	ND
206.1067	4.51	NA	NA	NA	NA	NA	High in infected	0.008	ND	ND
549.2233	2.49	NA	NA	NA	NA	NA	High in uninfected	0.008	ND	ND
522.2834	4.16	NA	NA	NA	NA	NA	High in infected	0.008	ND	High in infected ear center
303.2323	4.1	5,6-Epoy-8Z,11Z,14Z-eicosatrienoic acid	0	4	0.89	8	High in infected	0.008	High in infected ear center	No difference

										noted
327.2325	4.05	NA	NA	NA	NA	NA	High in infected	0.008	ND	ND

508.3764	4.01	PC(P-18:0/0:0)	0	2	0.91	10	High in infected	0.008	High in infected ear center	High in infected ear center
281.0052	2.55	NA	NA	NA	NA	NA	High in infected	0.008	Lowest in infected ear center compared to all other groups	No differencenoted
377.2661	4.32	NA	NA	NA	NA	NA	High in infected	0.008	Lower in infected ear center compared to all other groups	High in infected ear center
230.1756	2.74	NA	NA	NA	NA	NA	High in uninfected	0.008	No difference noted	ND

[1] Test returns identical p-values when non-overlapping peak areas are obtained between samples in each group (due to identical ranks regardless of the specific peak areas.)

[2] NA, not applicable

[3] ND, not detected

Table 4. Top differential molecules for footpad organic extraction as determined by random forest

m/z	**RT**	**Spectral match on GNPS / LIPID MAPS / Molecular networking**	**Mass difference**	**PPM error**	**Cosine score**	**Number of matched peaks**	**Impact of infection in footpad**	**P values [1]**	**Impact of infection in ear (Aqueous extraction)**	**Impact of infection in ear (Organic extraction)**
794.6035	5.97	PC O-38:5	0	3	0.81	7	High in infected	0.008	High in infected ear edge	High in infected ear center
768.5885	5.89	PC O-36:4	NA[2]	2.21	NA	NA	High in infected	0.008	ND	High in infected ear center
703.5752	4.7	NA	NA	NA	NA	NA	High in infected	0.008	High in infected ear center	High in infected ear center
720.5895	6.63	NA	NA	NA	NA	NA	High in infected	0.008	High in infected ear edge	High in infected ear center
796.6135	6.64	NA	NA	NA	NA	NA	High in infected	0.008	High in infected ear edge	ND
828.5521	5.36	NA	NA	NA	NA	NA	High in uninfected	0.008	ND	High in uninfected ear center

811.6686	6.55	SM 42:3;O2	NA	NA	NA	NA	High in infected	0.008	High in infected ear edge	ND
796.6182	6.59	PC(17:0/20:4)	0	3	0.8	6	High in infected	0.008	High in infected ear edge	ND
744.5891	6.01	PE(18:1/18:1)	0	4	0.76	13	High in infected	0.008	High in infected ear center	ND
352.2937	4.71	NA	NA	NA	NA	NA	High in infected	0.008	ND	High in infected ear center
519.4891	3.79	NA	NA	NA	NA	NA	High in infected	0.008	ND	ND
480.3097	2.81	PE(18:1(9Z)/0:0)	NA	NA	NA	NA	High in uninfected	0.008	No difference noted	Lowest in the infected ear center compared to all other groups
813.6867	7.51	SM(d18:1/22:0)	0	4	0.91	6	High in infected	0.008	ND	High in infected ear edge
585.534	3.53	NA	NA	NA	NA	NA	High in infected	0.016	High in infected ear center	ND
722.4983	7.85	NA	NA	NA	NA	NA	High in uninfected	0.095	ND	ND

[1] Test returns identical p-values when non-overlapping peak areas are obtained between samples in each group (due to identical ranks regardless of the specific peak areas.)
[2] NA, not applicable
[3] ND, not detected

Chapter 3: Discussion

The metabolome provides a link between genotype and phenotype, by identifying changes occurring at the molecular level, for example when parasites and their hosts interact [15]. Metabolism is also an indicator of the host physiological state. Understanding the infection-induced host metabolic alterations could lead to new treatments for parasitic diseases [16], particularly host-targeted drug therapy focused on pathways otherwise redundant to the host but important for parasite invasion, replication and survival [17], or on mitigating damage caused by the parasite [16]. In addition, changes in host plasma metabolite abundance, including pyruvate, taurine and *N*-acetylglutamine, can serve as an indicator of response to CL treatment [18]. Several studies have investigated *Leishmania* metabolism during *in vitro* macrophage infection (*e.g. [19]*), or in amastigotes purified from mouse granulomatous lesions [20], but there is still a lack of knowledge of host metabolic responses during *in vivo* infection. Given the relative host vs parasite biomass, the slow replication of *Leishmania* during *in vivo* infection [20], and the fact that lesion-derived amastigote PC composition significantly differs from mouse tissue PC composition [21] whereas most detected metabolites in our study are found in both infected and uninfected samples, it is likely that most metabolites identified in our study were host-derived, thereby expanding our understanding of host metabolic contributions to CL pathogenesis.

Amongst annotatable metabolites in our study, members of the PC family were most affected by infection in both intradermal ear infection and subcutaneous footpad infection models. PCs of the *m/z* range 200-799 and total PCs were significantly higher with infection at the site of infection (infected ear center) (Figure 1E-K). PCs were also increased in the infected footpad (Tables 3, 4, Figure S2). This increase concurs with prior reports of elevated lysophosphatidylcholine (LPC) and PCs in infected macrophages *in vitro* [22][23]. Concordance between infection models supports our approach and translatability of results.

LPC has immunomodulatory roles that promote parasite growth [24]. PCs elevation may also reflect increased membrane turnover during infection and modulate immune responses [25]. For example, PC biosynthesis is a critical component of Golgi membrane remodeling following TLR4 engagement, and is required for secretion of TNFα and interleukin 6 cytokines [26]. TLR4 is required for control of *L. major* infection [27]. Elevation of PCs is also a marker of switch from monocyte to macrophage [28]. Increased PCs may also reflect phagolysosome membranes given the intracellular lifestyle of *L. major [25]*, though PC elevation was also observed during infection with *T. cruzi,* which resides in the cytosol [29][30].

Miltefosine is a commonly administered oral drug for the treatment of visceral leishmaniasis and CL that targets the PC biosynthetic pathway, inhibiting phosphatidylethanolamine-N-methyltransferase and activating phospholipase A2 in *Leishmania* [31]. In mammalian cells, miltefosine also decreases phosphatidylethanolamine-N-methyltransferase activity, while also decreasing membrane-bound CTP:phosphocholine cytidylyltransferase activity, leading to reduced levels of PCs [32]. Thus, it may be expected to proceed via host-directed effects in addition to impacts on parasite metabolism [32]. This is further supported by recent observations that PC biosynthesis is dispensable in *Leishmania* amastigotes [21].We therefore speculate that miltefosine mechanism of action in CL may thus involve re-normalization of infection-induced changes in host PCs and restricting the parasite's

ability to scavenge host PCs. Future studies are thus needed to investigate the mechanism of action of miltefosine with respect to host metabolism in CL *in vivo*.

Additional annotatable infection-affected metabolites also included the omega-3 fatty acid eicosatrienoic acid and glutamine. Glutamine was significantly lower with infection at the site of the ear lesion. These findings contrast with metabolomic profiling of *L. amazonensis*-infected macrophages, which showed increased glutamine levels [33]. A recent study in mice infected with *L. donovani,* however, showed heightened glutamine consumption with infection and a role of glutamine supplementation in clearing parasite load [34]*,* which concur with our findings*.* Future studies should aim to look at the specific functional role of glutamine metabolism in *L. major* infection.

The clinical presentations of CL lesions can vary and lesions are capable of self-healing in some cases. However, resolving them can take several months to years, leaving a significant amount of scarring. In cases of Post-Kala Azar dermal leishmaniasis, patients can continue to serve as a reservoir for the parasites after the lesions have long been healed [35]. Our results showed significant perturbations in the metabolism of the skin lesions, with the area near the skin lesions also being affected in experimental CL. Our study relied on bioluminescence to measure parasite burden and as such we cannot ascertain whether parasites were still present at low levels in the sites adjacent to the skin lesions. There is therefore still a strong need to understand the role of lesion-free tissues in transmission of *Leishmania* and in disease pathogenesis. However, our results are consistent with findings of microbiota dysbiosis in lesion-adjacent tissues in humans and in lesion-free cutaneous sites in mice [36]

This study looked at both ear and footpad infection models, although the effect of infection on metabolism was found to be more minor in the footpad. Nevertheless, PC family metabolites were increased with infection in both sites, showcasing similarities in pathogenesis processes between these two infection models. These similarities are particularly striking given differences in pathogenic processes between ear and footpad models, including differences in elicited immune response [37][38] and vaccine-mediated protection [39].

While this untargeted metabolomics study enabled us to uncover several metabolic pathways affected in CL, on average compounds that couldn't be directly annotated (level 2 annotations according to metabolites standards initiative [40]) still represent 71.11% of our data. Molecular networking did enable us to extend annotations further, so that 64.44% of our top 15 most differential metabolite features identified by random forest had at least family-level (level 3) annotations [40]. Nevertheless, metabolomics annotation rates are continuously improving. Our results have been deposited in a "living data" database [14], where they are continuously being re-annotated as reference libraries and computational tools expand. As such, they will continue to yield expanding insights into CL pathogenesis and serve as a building point for expanded studies of metabolism in CL. Such results will help guide the next generation of CL drug treatments.

Chapter 4: Materials and Methods

In vivo experimentation

Female BALB/c mice (6-8 week-old) were injected intradermally in the left ear with $1x10^6$ luciferase-expressing *L. major* strain LV39 promastigotes (n=5) or in the left rear footpad with $5x10^6$ luciferase-expressing *L. major* strain LV39 promastigotes in PBS (n=5) [41]. These inocula were selected based on standard inocula for each model (see [42] and [43]). Infected and uninfected ear tissue, including the entirety of the lesion area ("infected ear center") and the entirety of the surrounding, macroscopically-healthy surrounding area ("infected ear edge"), as well as matched positions from the other, uninfected, ear ("uninfected ear center", "uninfected ear edge") were collected 8 weeks post-infection and immediately snap-frozen. Infected and uninfected footpads were collected 7 weeks post-infection; lesion tissue was scraped off above the footpad bones and collected in its entirety, with matched tissue collected from the other, uninfected, footpad. The entirety of the tissue was immediately snap-frozen. Samples were stored at -80°C until metabolite extraction. Parasites were maintained at 28 °C in M199 medium (Sigma) supplemented with 10% fetal bovine serum (Sigma), 1% penicillin-streptomycin, RPMI 1640 vitamin mix (1%), HEPES (25 mM), adenosine (100 µM), glutamine (1 mM), hemin (0.005%), $NaHCO_3$ (12 mM) and folic acid (10 µM) (pH 7.2) [44].

LC-MS/MS

Metabolite extraction, liquid chromatography and mass spectrometry were performed as previously described [45]. Briefly, metabolites were extracted by homogenization in a Tissuelyzer using a 5 mm stainless steel bead (Qiagen) in 50% methanol (aqueous extract) followed by 3:1 dichloromethane:methanol (organic extract). LC was performed on an UltiMate 3000 UHPLC (Thermo Scientific) with Phenomenex UHPLC 1.7 µm 100 Å Kinetex C8 column (50 X 2.1 mm), and with water and 0.1% formic acid as mobile phase A and acetonitrile and 0.1% formic acid as mobile phase B, flow rate of 0.5 mL/min and column temperature of 40°C. LC gradient parameters were optimized for each extraction with regards to overall chromatogram peak shape (Table 5). Daily MS calibration was performed with ESI-L Low Concentration Tuning Mix, which covers *m/z* 118.086 to 2721.895 (Agilent Technologies). The internal calibrant (lock mass) Hexakis(1H,1H,3H-tetrafluoropropoxy)phosphazene (Synquest Laboratories), *m/z* 922.009798, was present throughout the run, as previously described [45][46][47]. MS was performed in positive mode on a Maxis Impact HD QTOF mass spectrometer (Bruker); instrumental parameters are listed in Table 6. MS/MS data for each run was collected by fragmentation of the ten most intense ions, in range 80-2,000 *m/z*, with active exclusion after 4 spectra and release after 30s. Instrumental performance controls included solvent blanks, pooled quality controls for each tissue type and a standard mix of 6 molecules (sulfamethazine, sulfadimethoxine, sulfachloropyridazine, coumarin-314, sulfamethizole, amitriptyline). To further avoid any confounding from run order, we alternated between samples from infected and uninfected animals.

Table 5. LC gradient parameters.

Ear aqueous extraction	
Start	2% B

1 min	2% B
1.5 min	40% B
4 min	98% B
5 min	98% B
6 min	2% B
7 min	2% B
Ear organic extraction	
Start	2% B
1 min	2% B
1.5 min	60% B
5.5 min	98% B
7.5 min	98% B
8.5 min	2% B
10.5 min	2% B
Footpad aqueous extraction	
Start	2% B
1 min	2% B
1.5 min	40% B
6 min	98% B
6.5 min	98% B
7 min	2% B
Footpad organic extraction	
Start	2% B
1 min	2% B
1.5 min	70% B
7 min	98% B

8 min	98% B
9 min	2% B
10.5 min	2% B

Table 6. MS parameters

Detection mode	Positive
Nebulizer gas pressure	2 Bar
Capillary voltage	4,500 V
Ion source temperature	200°C
Dry gas flow	9.0 L/min
Spectra rate acquisition	3 spectra/s

LC-MS/MS Data analysis

LC-MS/MS data was processed using MZmine 2.37 [48], with parameters as shown in Table 7.

Table 7. MZmine parameters

Mass Detection	
MS level 1: Noise level	1.00E+03
MS level 2: Noise level	10
Mass detector	Centroid
Chromatogram Builder	
Min time span	0.06 min
Min peak height	3.00E+03
m/z tolerance	1e-6 or 10 ppm
Chromatogram deconvolution	
Algorithm	Baseline cutoff
Min peak height	3.00E+03
Peak duration range (min)	0.06-2 min (ear), 0.01-7 min (footpad)
Baseline level	1.00E+02 (ear), 1.50E+03 (footpad)
m/z range for MS2 scan pairing (Da)	0.01
RT range for MS2 scan pairing (min)	0.2 min
Isotopic Peaks Grouper	
m/z tolerance	1e-6 or 10 ppm
Retention time tolerance (absolute: min)	0.05 min
Monotonic shape	Enabled
Maximum charge	3
Representative isotope	Most intense

Join Aligner	
m/z tolerance	1e-6 or 10 ppm
Weight for m/z	7
Retention time tolerance (absolute: min)	0.5 min
Weight for RT	3
Manual filtering	
Min number of peaks per row	3
RT range	0.2-10.5 (ear organic and footpad), 0.2-6.9 (ear aqueous),
MS2	required
Manual validation of peak shape	
Gap-filing	
m/z tolerance	0.000001 or 10 ppm
RT tolerance	0.5 min
Intensity tolerance	30%
RT correction	Enabled

Features with peak area within 3-fold of peak area in blanks were removed. Normalization to total peak area (Total ion current (TIC) normalization) and data processing was performed in Jupyter notebook in R [49]. Principal Coordinate Analysis (PCoA) was done using the Bray-Curtis-Faith dissimilarity matrix implemented in QIIME1 [50] and PERMANOVA calculations were performed using the R package "vegan" to compare the chemical similarity of samples from the four groups of varying condition and position of infection [51,52]. EMPeror was used to visualize PCoA plots [53]. randomForest package in R was used to find variables of importance associated with infection and sampling conditions, using 7000 trees [13]. Global Natural Products Social Molecular Networking platform (GNPS) was used to annotate molecules from spectral library references and to perform feature-based molecular networking [14][54][55]. The following parameters were used in GNPS: precursor ion mass tolerance of 0.02 Da, fragment ion mass tolerance of 0.02 Da, minimum cosine score of 0.7 and 4 or more matched fragment ions. The maximum shift allowed between two MS/MS spectra was 500 Da, 10 maximum neighbor nodes allowed and maximum difference between precursor ion mass of searched MS/MS spectrum and library spectra was 100 Da. Spectral matches were evaluated by considering cosine scores, quality of mirror plots, as well as the number of matched peaks. Molecular network visualization was done in Cytoscape 3.7.2 [56]. All members of the PC subnetworks were visually inspected and verified to contain the diagnostic MS/MS peaks with *m/z* 184.08 (phosphocholine), *m/z* 125.00 (2,2-Dihydroxy-1,3,2-dioxaphospholan-2-ium) and *m/z* 86.10 (N,N,N-Trimethylethenaminium) from the phospholipid head group. Putative annotations for members of the PC subnetworks that were not available through spectral matching in GNPS were obtained using LipidMaps [57]. Notched box plots showing metabolite feature abundance for the four different groups (infected/uninfected vs. center/edge) for the ear samples and two different groups (infected vs. uninfected) for the footpad samples along with non-parametric two-tailed Wilcoxon statistical tests were both performed in R. Boxplot

whiskers represent the lowest and largest data points and non-overlapping boxplot notches indicate different medians between groups (95% confidence) [58].

Chapter 5: Supplemental information

Supplementary Materials:

Figure S1. Mirror plots for differential annotatable metabolites. (A) *m/z* 746.6052 RT 4.78 min, PC O-16:0/18:1.
(B) *m/z* 147.0815 RT 0.34 min, Glutamine.
(C) *m/z* 792.5574, RT 5.71 min, PC O-16:0/22:6.
(D) *m/z* 303.2323, RT 4.1 min, 5,6-Epoxy-8Z,11Z,14Z-eicosatrienoic acid from NIST14.
(E) *m/z* 508.3764, RT 4.01 min, PC P-18:0/0:0.

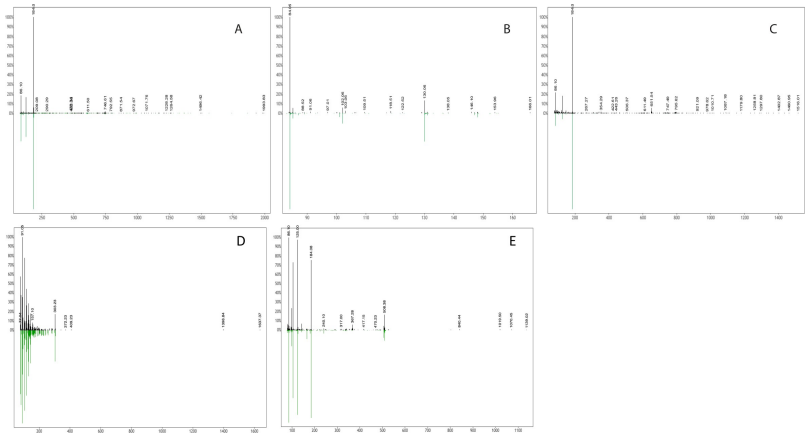

Figure S2 PC subnetworks. (A-D) PC family metabolites in the footpad organic, footpad aqueous, ear aqueous and ear organic molecular networks, respectively. Metabolite abundance in the presence of infection is shown in red and absence of infection is blue.

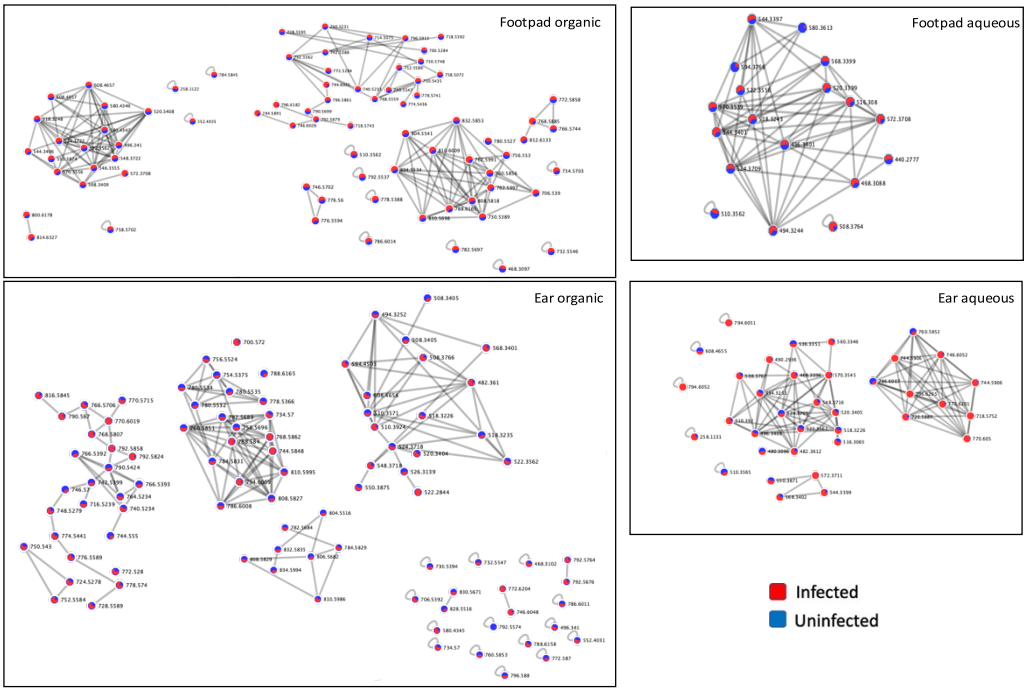

Table S1. All annotatable PC metabolites for ear organic extraction.

m/z	RT	GNPS/LIPID MAPS	Cosine score	Number of shared peaks	PPM error	Mass difference
468.3102	2.78	PC 14:0/18:0	0.96	11	1	0
482.361	3.04	PC O-16:0/0:0	0.81	6	2	0
494.3252	2.86	LPC 16:1 or LPC O-16:2;O *			2.23	
496.341	2.98	LPC 16:0	0.77	8	0	0.01
508.3405	2.94	PC P-18:0/0:0	0.91	10	3	0
508.3405	3.07	LPC 17:1 or LPC O-17:2;O *			0.27	
508.3766	3.12	PC P-18:0/0:0	0.91	10	3	0
510.3571	3.11	PC 17:0/0:0	0.93	9	0	0
510.3924	3.35	LPC O-18:0	0.79	6	2	0
518.3226	2.98	LPC 18:3 *			2.5	

518.3235	2.93	LPC 18:3 *			1.16	
520.3404	3	LPC 18:2 or LPC O-18:3;O *			1.15	
522.2844	3.02	LPC 17:2;O *			66.25	
522.3562	3.05	LPC 18:1	0.96	14	2	0
524.3718	3.59	LPC 18:0 or LPC O-18:1;O *			1.34	
526.3139	3.13	LPC 17:0;O *			69.16	
548.3718	3.31	LPC 20:2 or LPC O-20:3;O or PC O-20:2 *			1.28	
550.3875	3.31	LPC 20:1	0.95	16	0	0
552.4031	3.56	PC 20:0/0:0	0.91	11	1	0
568.3401	2.91	LPC 22:6 or PC O-22:6 *				
580.4345	3.93	PC 22:0/0:0	0.94	13	0	0
594.4503	4.17	LPC 23:0 or LPC O-23:1;O or PC O-23:0 *			1.68	
608.4658	4.42	LPC 24:0	0.93	13	1	0
700.572	5.25	LPC O-32:3 *				
706.5392	5.38	PC 14:0/16:0	0.97	8	0	0
716.5239	5.53	LPC 31:3;O *			1.95	
724.5278	5.71	LPC 33:5 or LPC O-33:6;O or PC O-33:5 *			2.3	
728.5589	6.4	LPC 33:3 *			0	
730.5394	5.14	PC 16:1/16:1	0.96	12	1	0
732.5547	5.5	PC 18:1/14:0	0.97	10	0	0
734.57	6.02	PC 14:0/18:0	0.99	15	0	0
734.57	8.81	PC 14:0/18:0	0.99	15	0	0
740.5234	5.4	LPC 33:5;O *			1.22	

742.5399	5.63	LPC 33:4;O or PC 33:3 or PC O-33:4;O *			0.31	
744.555	5.61	LPC 33:3;O or PC 33:2 or PC O-33:3;O *			0.16	
744.5848	5.59	LPC 34:2 or LPC O-34:3;O or PC O-34:2 *			7.25	
746.57	5.89	PC O-16:0/18:1	0.89	12	1	0
746.6048	8.81	PC O-16:0/18:1	0.93	12	3	0
748.5279	5.52	PC O-35:7 *			0.4	
750.543	5.79	PC O-35:6 *			1.75	
752.5584	6.29	PC O-35:5 *			0.66	
754.5375	5.48	LPC 34:5;O or PC 34:4 or PC O-34:5;O *			0.8	
756.5524	6.01	LPC 34:4;O or PC 34:3 or PC O-34:4;O *			1.85	
758.5696	5.62	PC 16:0/18:2	0.98	12	3	0
760.5851	6.15	PC 16:0/18:1	0.99	24	2	0
760.5853	8.8	PC 16:0/18:1	0.99	24	2	0
762.5986	8.8	LPC 34:1;O or PC 34:0 or PC O-34:1;O *			2.75	
762.5986	8.81	LPC 34:1;O	0.85	7	2	0
764.5234	5.38	PC 35:6 or PC O-35:7;O *			1.18	
766.5392	5.52	PC 35:5 or PC O-35:6;O *			1.44	
766.5393	5.54	PC 35:5 or PC O-35:6;O *			1.57	
766.5706	5.78	PC O-36:5	0.92	9	1	0
768.5807	5.74	PC O-36:4 *			12.36	
768.584	5.73	PC O-36:4 *			8.07	
768.5862	5.26	PC O-36:4 *			5.2	
770.5715	5.46	PC 35:3 or PC O-35:4;O *			2.73	

770.6019	5.7	PC O-36:3 *			5.06	
772.528	5.72	PC O-37:9 *			0.52	
772.587	5.91	PC P-18:0/18:1	0.92	9	1	0
772.6204	8.81	PC O-36:2 *			1.42	
774.5441	5.65	PC O-37:8 *			1.16	
776.5589	6.06	PC O-37:7 *			0	
778.5366	5.24	PC 36:6	0.95	8	0	0
778.574	6.27	PC O-37:6 *			0.64	
780.5532	5.59	PC 36:5 or PC O-36:6;O *			0.77	
780.5534	5.55	PC 36:5 or PC O-36:6;O *			0.51	
780.5535	5.59	PC 36:5 or PC O-36:6;O *			0.38	
782.5684	8.76	PC 18:2/18:2	0.99	19	2	0
782.5689	5.52	PC 18:2/18:2	0.99	19	2	0
784.5829	8.79	Spectral Match to Arachidonoylthio-PC	0.89	6	1	0
784.5831	5.72	PC 36:3	0.95	10	1	0
786.6008	6.32	PC 18:0/18:2	0.98	19	4	0
786.6011	8.8	PC 18:0/18:2	0.98	19	4	0
788.6158	8.81	PC 18:0/18:1	0.95	7	5	0
788.6165	4.85	PC 36:1 or PC O-36:2;O *			0.13	
790.5424	5.43	PC 37:7 or PC O-37:8;O *			5.44	
790.567	5.61	PC O-38:7 *			9.49	
792.5574	5.72	PC O-16:0/22:6	0.86	7	8	0.01
792.5676	5.75	PC O-16:0/22:6	0.87	7	20	0.02

792.5764	5.75	PC O-16:0/22:6	0.92	14	9	0.01
792.5824	5.67	PC O-38:6	0.92	14	9	0.01
792.5858	5.69	PC O-38:6	0.94	13	3	0
794.6009	5.88	PC O-38:5 *			6.17	
796.588	5.84	PC 37:4 or PC O-37:5;O *			3.64	
804.5516	5.53	PC 38:7 or PC O-38:8;O *			4.82	
806.5682	5.42	PC 38:6 or PC O-38:7;O *			1.49	
808.5827	5.61	PC 38:5 or PC O-38:6;O *			2.97	
808.5829	8.75	PC 38:5 or PC O-38:6;O *			2.72	
810.5986	8.76	PC 18:0/20:4	0.98	15	0	0
810.5995	6.12	PC 18:0/20:4	0.98	15	0	0
816.5845	5.6	PC O-40:8 *			6.98	
828.5516	5.44	PC O-40:10;O or PC 40:9 *			1.2	
830.5671	5.35	PC 20:4/20:4	0.78	8	3	0
832.5835	5.48	PC 40:7 or PC O-40:8;O *			0	
834.5994	5.91	PC 40:6 or PC O-40:7;O *			1.56	

Table S2. All annotatable PC metabolites for ear aqueous extraction.

m/z	RT	GNPS/LIPID MAPS	Cosine score	Number of shared peaks	PPM error	Mass difference
258.11131	0.37	alpha-GPC	0.86	5	8	0

468.3096	3.28	PC 14:0/18:0	0.98	15	2	0
480.3096	3.5	LPC 15:1 or LPC O-15:2;O *			2.29	
482.3612	3.53	PC O-16:0/0:0	0.76	10	2	0
490.2936	3.2	LPC 16:3 or LPC O-16:4;O *			1.63	
494.3251	3.36	LPC 16:1 or LPC O-16:2;O *			2.02	
496.3408	3.48	LPC 16:0 or LPC O-16:1;O *			2.02	
508.3767	3.57	PC P-18:0/0:0	0.94	9	3	0
510.3565	3.58	LPC 17:0	0.91	8	0	0
510.3992	3.79	LPC O-18:0	0.79	7	1	0
516.3065	3.34	LPC 18:4 or LPC O-18:5;O *			3.87	
518.3226	3.48	LPC 18:3 or LPC O-18:4;O *			2.89	

520.3405	3.38	LPC 18:2 or LPC O-18:3;O *			1.35	
522.3561	3.54	LPC 18:1	0.99	18	0	0
524.3709	3.7	PC 18:0/0:0	0.96	14	0	0
536.3351	3	LPC 18:2;O *			0.75	
544.3399	3.43	LPC 20:4 or LPC O-20:5;O *			0.18	
548.3716	3.61	LPC 20:2 or LPC O-20:3;O *			0.91	
550.3871	3.77	LPC 20:1	0.87	13	0	0
560.3346	3.13	LPC 20:4;O or PC 20:3 or PC O-20:4;O *			0.18	
568.3402	3.41	LPC 22:6 or PC O-22:6 *			0.7	
570.3545	3.5	LPC 22:5 or LPC O-22:6;O or PC O-22:5 *			1.58	
572.3	3.59	LPC 22:4 or LPC O-22:5;O or PC O-22:4 *			0	

711						
608.4655	4.44	LPC 24:0	0.92	12	0	0
718.5752	6.13	LPC 32:1 or LPC O-32:2;O or PC O-32:1 *			0.97	
720.5887	4.7	LPC 32:0 or LPC O-32:1;O or PC O-32:0 *			2.08	
744.5906	4.48	LPC 34:2 or LPC O-34:3;O or PC O-34:2 *			0.54	
744.5906	6.16	LPC 34:2 or LPC O-34:3;O or PC O-34:2 *			0.54	
746.6052	4.78	PC O-16:0/18:1	0.96	14	4	
760.5852	4.6	PC 16:0/18:1	0.98	13	2	0
770.605	4.58	PC O-36:3 *			1.04	
772.6201	4.7	PC O-36:2 *			1.81	
786.6007	4.65	PC 18:0/18:2	0.97	16	4	0
794.6	4.42	PC 20:3/18:1	0.82	5	0	0

051						
794.6052	6.13	PC 20:3/18:1	0.76	5	0	0
796.6205	4.91	PC O-38:4 *			1.26	

Table S3. All annotatable PC metabolites for footpad organic extraction.

m/z	RT	GNPS/LIPID MAPS	Cosine score	Number of shared peaks	PPM error	Mass difference
258.1122	0.3	alpha-GPC	0.85	5	4	0
468.3097	2.61	LPC 14:0	0.96	13	2	0
496.341	2.77	LPC 16:0 *			2.42	
510.3562	2.84	PC 17:0/0:0	0.94	12	1	0
518.3248	2.7	LPC 18:3 *			1.35	
520.3408	2.72	LPC 18:2			1.92	
522.3562	2.79	LPC 18:1	0.99	19	0	0
524.3722	2.96	PC 18:0/0:0	0.97	14	2	0
544.3406	2.7	LPC 20:4 *			1.47	

546.3555	2.77	LPC 20:3 *			0.18	
548.3722	2.83	LPC 20:2 *			2.01	
550.3874	3.04	LPC 20:1	0.96	14	0	0
552.4035	3.24	LPC 20:0	0.95	13	0	0
568.3409	2.7	LPC 22:6 *			1.94	
570.3556	2.78	LPC 22:5 or LPC O-22:6;O or PC O-22:5 *			0.35	
572.3708	2.83	LPC 22:4 or LPC O-22:5;O or PC O-22:4 *			0.52	
580.4346	3.58	PC 22:0/0:0	0.97	14	0	0
580.4347	3.58	LPC 22:0	0.97	14	0	0
608.4657	4.05	PC 24:0/0:0	0.96	14	1	0
608.4657	4.05	Lyso PC 24:0	0.96	14	1	0
700.5284	5.81	LPC 31:3 *			1.14	
706.539	5.3	PC 14:0/16:0	0.99	8	0	0
714.5075	5	LPC 31:4;O or PC 31:3 or PC O-31:4;O *			0.98	

718.5392	6.02	LPC 31:2;O or PC 31:1 or PC O-31:2;O *			1.53	
718.5743	5.89	LPC 32:1 *			0.28	
720.5547	5.65	LPC 31:1;O *			1.25	
728.5595	6.46	LPC 33:3 *			0.82	
730.5389	4.98	PC 16:1/16:1	0.99	16	1	0
730.5748	7.13	LPC 33:2 pr LPC O-33:3;O or PC O-33:2 *			0.41	
732.5546	5.48	PC 14:0/18:1	0.97	12	0	0
734.5703	6.04	PC 14:0/18:0	0.97	11	0	0
738.5072	4.97	LPC 33:6;O or PC 33:5 or PC O-33:6;O *			0.54	
740.5231	5.37	LPC 33:5;O *			0.81	
740.5233	5.14	LPC 33:5;O or PC 33:4 or PC O-33:5;O *			1.08	
742.5388	5.64	LPC 33:4;O or PC 33:3 or PC O-33:4;O *			0.94	
744.5551	6.17	LPC 33:3;O *			1.75	
744.5891	6.01	LPC 34:2 or LPC O-34:3;O or PC O-34:2 *			1.48	

746.5702	5.89	PC O-16:0/18:1	0.92	8	5	0
746.6026	6.79	PC O-16:0/18:1	0.95	18	0	0
750.5435	5.88	PC O-35:6 *			0.4	
752.5589	6.39	PC O-35:5 *			0	
756.553	6.05	LPC 34:4;O or PC 34:3 or PC O-34:4;O *			1.06	
758.5702	5.59	16:0-18:2 PC	0.92	12	2	0
760.5856	6.17	PC 18:1/16:0	0.99	18	4	0
762.5991	7.04	LPC 34:1;O *			2.1	
762.5997	7.1	PC 34:0 *			1.31	
766.5744	5.82	PC O-36:5	0.96	15	3	0
768.5559	6.1	PC 35:4 *			2.73	
768.5885	5.89	PC O-36:4 *			2.21	
772.5284	5.25	PC O-37:9 *			1.04	
772.5858	5.96	PC P-18:0/18:1	0.95	8	0	0

774.5436	5.66	PC O-37:8 *			0.52	
776.5594	6.21	PC O-37:7 *			0.64	
776.56	6.11	PC O-37:7 *			1.42	
778.5388	4.78	PC 18:3/18:3	0.95	8	3	0
778.5741	6.33	PC O-37:6 *			0.51	
780.5527	5.62	PC 36:5/PC O-36:6;O *			1.41	
782.5697	5.49	PC 16:0/18:1	0.98	20	0	0
784.5845	5.77	Arachidonoylthio-PC	0.94	8	0	0
786.6014	6.35	PC 18:0/18:2	0.98	23	0	0
788.6165	7.16	PC 18:0/18:1	0.95	7	5	0
790.5699	5.59	PC O-38:7 *			5.82	
792.5537	5.3	PC O-16:0/22:6	0.91	7	3	0
792.5562	5.92	PC O-16:0/22:6	0.91	7	3	0
792.5879	5.72	PC O-16:0/22:6	0.97	16	2	0

794.6035	5.97	PC O-38:5 *			2.9	
796.5861	5.88	PC 37:4 *			1.26	
796.5913	6.61	PC 37:4 *			7.78	
796.6182	6.59	PC O-38:4 *			4.14	
800.6178	6.85	PC 37:2 or PC O-37:3;O *			1.75	
804.5534	5.13	PC 38:7 *			0.5	
804.5541	4.94	PC 38:7 *			0.37	
808.5818	5.41	PC 38:5 *			4.08	
810.6009	6.24	PC 18:0/20:4	0.99	14	2	0
812.6133	6.3	PC 38:3 *			3.82	
814.6327	7.48	PC 38:2/PC O-38:3;O *			0.86	
830.5698	5.07	PC 20:4	0.91	17	6	0.01
832.5853	5.5	PC 40:7 *			0.24	

Table S4. All annotatable PC metabolites for footpad aqueous extraction.

m/z	RT	GNPS/LIPID MAPS	Cosine score	Number of shared peaks	PPM error	Mass difference
440.2777	3.21	LPC 12:0	0.9	5	0	0
468.3088	3.4	LPC 14:0	0.97	15	4	0
494.3244	3.64	LPC 16:1 or LPC O-16:2;O *			0.61	
496.3401	3.82	LPC 16:0	0.86	9	22	0.01
508.3764	4.01	PC P-18:0/0:0	0.91	10	2	0
510.3562	4.03	LPC 17:0	0.92	9	1	0
516.308	3.46	LPC 18:4 or LPC O-18:5;O *			0.97	
518.3243	3.52	LPC 18:3 or LPC O-18:4;O *			0.39	
520.3399	3.68	LPC 18:2 or LPC O-18:3;O *			0.19	
522.3556	3.92	LPC 18:1 or LPC O-18:2;O *			0.38	
524.3709	4.18	LPC 18:0	0.97	15	0	0
544.3397	3.72	LPC 20:4 or LPC O-20:5;O or PC O-20:4 *			0.18	
544.3401	3.67	LPC 20:4 or LPC O-20:5;O or PC O-20:4 *			0.55	
568.3399	3.67	LPC 22:6 or PC O-22:6 *			0.18	
570.3539	3.83	LPC 22:5 or LPC O-22:6;O or PC O-22:5 *			2.63	
572.3708	3.95	LPC 22:4 or LPC O-22:5;O or PC O-22:4 *			0.52	
580.3613	3.98	PC 20:1;O *			0.69	
594.3766	4.1	PC 21:1;O *			0.17	

Funding: Data collection was supported by a postdoctoral fellowship from the Canadian Institutes of Health Research, award number 338511 to L-IM (www.cihr-irsc.gc.ca/). Work in

the McCall laboratory at the University of Oklahoma is supported by start-up funds from the University of Oklahoma (http://www.ou.edu/). This work was also partially supported by US National Institutes of Health (NIH) grant 5P41GM103484-07 to PCD (www.nih.gov/). We further acknowledge NIH Grant GMS10RR029121 (www.nih.gov/) and Bruker (www.bruker.com/) for the shared instrumentation infrastructure that enabled this work (to PCD). The funders had no role in study design, data collection and analysis, decision to publish, or preparation of the manuscript.

Institutional Review Board Statement: All vertebrate animal studies were performed in accordance with the USDA Animal Welfare Act and the Guide for the Care and Use of Laboratory Animals of the National Institutes of Health, under a protocol approved by the University of California San Diego Institutional Animal Care and Use Committee (S14187).

Data Availability Statement: Data has been deposited in MassIVE (massive.ucsd.edu, accession numbers MSV000081004 (ear) and MSV000080239 (footpad)). Molecular networking can be accessed here:
https://gnps.ucsd.edu/ProteoSAFe/status.jsp?task=451754c383de461e9e4abdf6eb3199d2 (aqueous ear extraction),
https://gnps.ucsd.edu/ProteoSAFe/status.jsp?task=0d092bbb213347c3bd7a19b9cae2bcf4 (organic ear extraction),
https://gnps.ucsd.edu/ProteoSAFe/status.jsp?task=eccdfd5f15be491b8993084c010467ef (aqueous footpad extraction),
https://gnps.ucsd.edu/ProteoSAFe/status.jsp?task=ecc0d126d74f4e6e8e3d599296d8f6e2 (organic footpad extraction).

Acknowledgments: Luciferase-expressing *L. major* parasites were provided by Dr. Martin Olivier, McGill University.

Conflicts of Interest: The authors declare no conflict of interest. The funders had no role in the design of the study; in the collection, analyses, or interpretation of data; in the writing of the manuscript, or in the decision to publish the results.

References

1. Georgiadou, S.P.; Makaritsis, K.P.; Dalekos, G.N. Leishmaniasis revisited: Current aspects on epidemiology, diagnosis and treatment. J Transl Int Med 2015, 3, 43–50.
2. Alvar, J.; Yactayo, S.; Bern, C. Leishmaniasis and poverty. Trends in Parasitology 2006, 22, 552–557.
3. Bern, C.; Maguire, J.H.; Alvar, J. Complexities of assessing the disease burden attributable to leishmaniasis. PLoS Negl. Trop. Dis. 2008, 2, e313.
4. Leishmaniasis Available online: https://www.who.int/leishmaniasis/disease/clinical_forms_leishmaniases/en/ (accessed on Jan 20, 2020).
5. McCall, L.-I.; Zhang, W.-W.; Matlashewski, G. Determinants for the Development of Visceral Leishmaniasis Disease. PLoS Pathog. 2013, 9, e1003053.
6. McCall, L.-I.; McKerrow, J.H. Determinants of disease phenotype in trypanosomatid parasites. Trends Parasitol. 2014, 30, 342–349.
7. Parasites-Leishmaniasis Available online: https://www.cdc.gov/parasites/leishmaniasis/biology.html (accessed on Jan 20, 2020).
8. Ponte-Sucre, A.; Gamarro, F.; Dujardin, J.-C.; Barrett, M.P.; López-Vélez, R.; García-Hernández, R.; Pountain, A.W.; Mwenechanya, R.; Papadopoulou, B. Drug resistance and treatment failure in leishmaniasis: A 21st century challenge. PLoS Negl. Trop. Dis. 2017, 11, e0006052.
9. Bueno-Marí, R.; Jiménez-Peydró, R. Global change and human vulnerability to vector-borne diseases. Front. Physiol. 2013, 4, 158.
10. Deidda, M.; Piras, C.; Bassareo, P.P.; Dessalvi, C.C.; Mercuro, G. Metabolomics, a promising approach to translational research in cardiology. IJC Metabolic & Endocrine 2015, 9, 31–38.
11. Vinayavekhin, N.; Saghatelian, A. Untargeted Metabolomics. Current Protocols in Molecular Biology 2010.
12. Vincent, I.M.; Weidt, S.; Rivas, L.; Burgess, K.; Smith, T.K.; Ouellette, M. Untargeted metabolomic analysis of miltefosine action in Leishmania infantum reveals changes to the internal lipid metabolism. Int. J. Parasitol. Drugs Drug Resist. 2014, 4, 20–27.
13. Breiman, L. Random Forests. Mach. Learn. 2001, 45, 5–32.
14. Wang, M.; Carver, J.J.; Phelan, V.V.; Sanchez, L.M.; Garg, N.; Peng, Y.; Nguyen, D.D.; Watrous, J.; Kapono, C.A.; Luzzatto-Knaan, T.; et al. Sharing and community curation of mass spectrometry data with Global Natural Products Social Molecular Networking. Nat. Biotechnol. 2016, 34, 828–837.
15. Newsom, S.N.; McCall, L.-I. Metabolomics: Eavesdropping on silent conversations between hosts and their unwelcome guests. PLoS Pathog. 2018, 14, e1006926.
16. Hossain, E.; Khanam, S.; Wu, C.; Lostracco-Johnson, S.; Thomas, D.; Katemauswa, M.; Gosmanov, C.; Li, D.; Woelfel-Monsivais, C.; Sankaranarayanan, K.; et al. 3D mapping of host-parasite-microbiome interactions reveals metabolic determinants of tissue tropism and disease tolerance in Chagas disease.

17. Varikuti, S.; Jha, B.K.; Volpedo, G.; Ryan, N.M.; Halsey, G.; Hamza, O.M.; McGwire, B.S.; Satoskar, A.R. Host-Directed Drug Therapies for Neglected Tropical Diseases Caused by Protozoan Parasites. Front. Microbiol. 2018, 9, 2655.
18. Vargas, D.A.; Prieto, M.D.; Martínez-Valencia, A.J.; Cossio, A.; Burgess, K.E.V.; Burchmore, R.J.S.; Gómez, M.A. Pharmacometabolomics of Meglumine Antimoniate in Patients With Cutaneous Leishmaniasis. Front. Pharmacol. 2019, 10, doi:10.3389/fphar.2019.00657.
19. Saunders, E.C.; Ng, W.W.; Kloehn, J.; Chambers, J.M.; Ng, M.; McConville, M.J. Induction of a Stringent Metabolic Response in Intracellular Stages of Leishmania mexicana Leads to Increased Dependence on Mitochondrial Metabolism. PLoS Pathog. 2014, 10, e1003888.
20. Kloehn, J.; Saunders, E.C.; O'Callaghan, S.; Dagley, M.J.; McConville, M.J. Characterization of metabolically quiescent Leishmania parasites in murine lesions using heavy water labeling. PLoS Pathog. 2015, 11, e1004683.
21. Moitra, S.; Basu, S.; Pawlowic, M.; Hsu, F.-F.; Zhang, K. De novo synthesis of phosphatidylcholine is essential for the promastigote but not amastigote stage in Leishmania major. Cold Spring Harbor Laboratory 2020, 2020.12.30.424847.
22. Henriques, C.; Atella, G.C.; Bonilha, V.L.; de Souza, W. Biochemical analysis of proteins and lipids found in parasitophorous vacuoles containing Leishmania amazonensis. Parasitol. Res. 2003, 89, 123–133.
23. Negrão, F.; Abánades, D.R.; Jaeeger, C.F.; Rocha, D.F.O.; Belaz, K.R.A.; Giorgio, S.; Eberlin, M.N.; Angolini, C.F.F. Lipidomic alterations of in vitro macrophage infection by L. infantum and L. amazonensis. Mol. Biosyst. 2017, 13, 2401–2406.
24. Tounsi, N.; Meghari, S.; Moser, M.; Djerdjouri, B. Lysophosphatidylcholine exacerbates Leishmania major-dendritic cell infection through interleukin-10 and a burst in arginase1 and indoleamine 2,3-dioxygenase activities. International Immunopharmacology 2015, 25, 1–9.
25. Bohdanowicz, M.; Grinstein, S. Role of phospholipids in endocytosis, phagocytosis, and macropinocytosis. Physiol. Rev. 2013, 93, 69–106.
26. Tian, Y.; Pate, C.; Andreolotti, A.; Wang, L.; Tuomanen, E.; Boyd, K.; Claro, E.; Jackowski, S. Cytokine secretion requires phosphatidylcholine synthesis. J. Cell Biol. 2008, 181, 945–957.
27. Kropf, P.; Freudenberg, M.A.; Modolell, M.; Price, H.P.; Herath, S.; Antoniazi, S.; Galanos, C.; Smith, D.F.; Müller, I. Toll-like receptor 4 contributes to efficient control of infection with the protozoan parasite Leishmania major. Infect. Immun. 2004, 72, 1920–1928.
28. Ecker, J.; Liebisch, G.; Englmaier, M.; Grandl, M.; Robenek, H.; Schmitz, G. Induction of fatty acid synthesis is a key requirement for phagocytic differentiation of human monocytes. Proc. Natl. Acad. Sci. U. S. A. 2010, 107, 7817–7822.
29. Hoffman, K.; Liu, Z.; Hossain, E.; Bottazzi, M.E.; Hotez, P.; Jones, K.; McCall, L.-I. Alterations to the cardiac metabolome induced by chronic T. cruzi infection relate to the degree of cardiac pathology. Cold Spring Harbor Laboratory 2020, 2020.09.17.300608.
30. Dean, D.A.; Gautham; Siqueira-Neto, J.L.; McKerrow, J.H.; Dorrestein, P.C.; McCall, L.-I. Spatial metabolomics identifies localized chemical changes in heart tissue during chronic cardiac Chagas disease. Cold Spring Harbor Laboratory 2020, 2020.06.29.178038.
31. Rakotomanga, M.; Blanc, S.; Gaudin, K.; Chaminade, P.; Loiseau, P.M. Miltefosine affects lipid metabolism in Leishmania donovani promastigotes. Antimicrob. Agents Chemother. 2007, 51, 1425–1430.

32. Jiménez-López, J.M.; Ríos-Marco, P.; Marco, C.; Segovia, J.L.; Carrasco, M.P. Alterations in the homeostasis of phospholipids and cholesterol by antitumor alkylphospholipids. Lipids Health Dis. 2010, 9, 33.
33. Muxel, S.M.; Mamani-Huanca, M.; Aoki, J.I.; Zampieri, R.A.; Floeter-Winter, L.M.; López-Gonzálvez, Á.; Barbas, C. Metabolomic Profile of BALB/c Macrophages Infected with Leishmania amazonensis: Deciphering L-Arginine Metabolism. International Journal of Molecular Sciences 2019, 20, 6248.
34. Ferreira, C.; Mesquita, I.; Barbosa, A.M.; Osório, N.S.; Torrado, E.; Beauparlant, C.-J.; Droit, A.; Cunha, C.; Carvalho, A.; Saha, B.; et al. Glutamine supplementation improves the efficacy of miltefosine treatment for visceral leishmaniasis. PLoS Negl. Trop. Dis. 2020, 14, e0008125.
35. Scorza, B.M.; Carvalho, E.M.; Wilson, M.E. Cutaneous Manifestations of Human and Murine Leishmaniasis. Int. J. Mol. Sci. 2017, 18, doi:10.3390/ijms18061296.
36. Gimblet, C.; Meisel, J.S.; Loesche, M.A.; Cole, S.D.; Horwinski, J.; Novais, F.O.; Misic, A.M.; Bradley, C.W.; Beiting, D.P.; Rankin, S.C.; et al. Cutaneous Leishmaniasis Induces a Transmissible Dysbiotic Skin Microbiota that Promotes Skin Inflammation. Cell Host Microbe 2017, 22, 13–24.e4.
37. Loeuillet, C.; Bañuls, A.-L.; Hide, M. Study of Leishmania pathogenesis in mice: experimental considerations. Parasit. Vectors 2016, 9, 144.
38. Ribeiro-Gomes, F.L.; Roma, E.H.; Carneiro, M.B.H.; Doria, N.A.; Sacks, D.L.; Peters, N.C. Site-dependent recruitment of inflammatory cells determines the effective dose of Leishmania major. Infect. Immun. 2014, 82, 2713–2727.
39. Tabbara, K.S.; Peters, N.C.; Afrin, F.; Mendez, S.; Bertholet, S.; Belkaid, Y.; Sacks, D.L. Conditions influencing the efficacy of vaccination with live organisms against Leishmania major infection. Infect. Immun. 2005, 73, 4714–4722.
40. Sumner, L.W.; Amberg, A.; Barrett, D.; Beale, M.H.; Beger, R.; Daykin, C.A.; Fan, T.W.-M.; Fiehn, O.; Goodacre, R.; Griffin, J.L.; et al. Proposed minimum reporting standards for chemical analysis Chemical Analysis Working Group (CAWG) Metabolomics Standards Initiative (MSI). Metabolomics 2007, 3, 211–221.
41. Roy, G.; Dumas, C.; Sereno, D.; Wu, Y.; Singh, A.K.; Tremblay, M.J.; Ouellette, M.; Olivier, M.; Papadopoulou, B. Episomal and stable expression of the luciferase reporter gene for quantifying Leishmania spp. infections in macrophages and in animal models. Mol. Biochem. Parasitol. 2000, 110, 195–206.
42. Côrtes, D.F.; Carneiro, M.B.H.; Santos, L.M.; Souza, T.C. de O.; Maioli, T.U.; Duz, A.L.C.; Ramos-Jorge, M.L.; Afonso, L.C.C.; Carneiro, C.; Vieira, L.Q. Low and high-dose intradermal infection with Leishmania majorand Leishmania amazonensis in C57BL/6 mice. Mem. Inst. Oswaldo Cruz 2010, 105, 736–745.
43. Zhang, W.W.; Ramasamy, G.; McCall, L.-I.; Haydock, A.; Ranasinghe, S.; Abeygunasekara, P.; Sirimanna, G.; Wickremasinghe, R.; Myler, P.; Matlashewski, G. Genetic analysis of Leishmania donovani tropism using a naturally attenuated cutaneous strain. PLoS Pathog. 2014, 10, e1004244.
44. McCall, L.-I.; El Aroussi, A.; Choi, J.Y.; Vieira, D.F.; De Muylder, G.; Johnston, J.B.; Chen, S.; Kellar, D.; Siqueira-Neto, J.L.; Roush, W.R.; et al. Targeting Ergosterol Biosynthesis in

Leishmania donovani: Essentiality of Sterol 14alpha-demethylase. PLOS Neglected Tropical Diseases 2015, 9, e0003588.
45. McCall, L.-I.; Morton, J.T.; Bernatchez, J.A.; de Siqueira-Neto, J.L.; Knight, R.; Dorrestein, P.C.; McKerrow, J.H. Mass Spectrometry-Based Chemical Cartography of a Cardiac Parasitic Infection. Anal. Chem. 2017, 89, 10414–10421.
46. Melnik, A.V.; Vázquez-Baeza, Y.; Aksenov, A.A.; Hyde, E.; McAvoy, A.C.; Wang, M.; da Silva, R.R.; Protsyuk, I.; Wu, J.V.; Bouslimani, A.; et al. Molecular and Microbial Microenvironments in Chronically Diseased Lungs Associated with Cystic Fibrosis. mSystems 2019, 4, doi:10.1128/mSystems.00375-19.
47. Quinn, R.A.; Melnik, A.V.; Vrbanac, A.; Fu, T.; Patras, K.A.; Christy, M.P.; Bodai, Z.; Belda-Ferre, P.; Tripathi, A.; Chung, L.K.; et al. Global chemical effects of the microbiome include new bile-acid conjugations. Nature 2020, 579, 123–129.
48. Pluskal, T.; Castillo, S.; Villar-Briones, A.; Orešič, M. MZmine 2: Modular framework for processing, visualizing, and analyzing mass spectrometry-based molecular profile data. BMC Bioinformatics 2010, 11.
49. Perez, F.; Granger, B.E. IPython: A System for Interactive Scientific Computing. Computing in Science & Engineering 2007, 9, 21–29.
50. Caporaso, J.G.; Kuczynski, J.; Stombaugh, J.; Bittinger, K.; Bushman, F.D.; Costello, E.K.; Fierer, N.; Peña, A.G.; Goodrich, J.K.; Gordon, J.I.; et al. QIIME allows analysis of high-throughput community sequencing data. Nat. Methods 2010, 7, 335–336.
51. Bray, J.R.; Roger Bray, J.; Curtis, J.T. An Ordination of the Upland Forest Communities of Southern Wisconsin. Ecological Monographs 1957, 27, 325–349.
52. Faith, D.P.; Minchin, P.R.; Belbin, L. Compositional dissimilarity as a robust measure of ecological distance. Theory and models in vegetation science 1987, 57–68.
53. Vázquez-Baeza, Y.; Pirrung, M.; Gonzalez, A.; Knight, R. EMPeror: a tool for visualizing high-throughput microbial community data. Gigascience 2013, 2, 16.
54. Phelan, V.V. Feature-Based Molecular Networking for Metabolite Annotation. Computational Methods and Data Analysis for Metabolomics 2020, 227–243.
55. Nothias Louis Felix Feature-based Molecular Networking in the GNPS Analysis Environment. BioRXiv 2019, doi:10.1101/812404.
56. Shannon, P.; Markiel, A.; Ozier, O.; Baliga, N.S.; Wang, J.T.; Ramage, D.; Amin, N.; Schwikowski, B.; Ideker, T. Cytoscape: a software environment for integrated models of biomolecular interaction networks. Genome Res. 2003, 13, 2498–2504.
57. Fahy, E.; Sud, M.; Cotter, D.; Subramaniam, S. LIPID MAPS online tools for lipid research. Nucleic Acids Res. 2007, 35, W606–12.
58. Chambers, J.M. Graphical methods for data analysis; Wadsworth International Group, 1983; ISBN 9780534980528.